EXPERIMENTS ON THE STATIC STABILITY OF A CHANGING CAPSULE SHAPE IN HYPERSONIC FLOW

P. M. Seltner[(1)], D. Neeb[(1)], A. Gülhan[(1)], L. Ferracina[(2)]

[(1)] German Aerospace Center (DLR), Supersonic and Hypersonic Technology Department of the Institute of Aerodynamics and Flow Technology, Linder Hoehe, 51147 Cologne, Germany, Email: Patrick.Seltner@dlr.de, Dominik.Neeb@dlr.de, Ali.Guelhan@dlr.de

[(2)] ATG Europe B.V. on behalf of the European Space Agency (ESA), Nordwijk, Netherlands, Email: Luca.Ferracina@esa.int

ABSTRACT

Capsule-like shapes are commonly used for Earth return or exploration missions, which experience very high velocities during atmospheric entry. For some of these missions such as sample return, neither aerodynamic stabilizers, like parachutes, nor RCS devices are employed. Therefore, the capsule stability has to be guaranteed solely by the spacecraft configuration in the complete flight regime from hypersonic to subsonic conditions. This very challenging task requires reliable design tools. However, both experimental and numerical approaches still exhibit shortcomings in fully modelling the flight environment. Hence, complementary applications are essential to improve these tools.

Ablative thermal protection systems are used for most of the exploration missions, that experience shape changes during the hypersonic flight. This may lead to a change of the pressure distribution as well as a displacement of the vehicle's centre of gravity. Since no control devices are available, the vehicle can become aerodynamically unstable, which may jeopardize the mission. State-of-the-art tools are not able to predict the recession of the Thermal Protection System (TPS) over the complete surface. As a consequence, it is typically considered in the margin policy of the aerodynamic design, which is why flight qualities and risks need to be analysed prior to flight.

As part of the ESA TRP MODSHAPE, experimental studies were performed to investigate the impact of a changing shape on the static stability of a capsule model. A modified Hayabusa model with camphor-coated front-shield is exposed to a hypersonic flow in order to enable sublimation along the coating. Tests were performed in the hypersonic wind tunnel H2K at the German Aerospace Center (DLR) in Cologne at flight relevant inflow conditions and two different angles of incident. Two in-situ and two ex-situ techniques for the front-shield recession measurements, a six-component balance for force/moment measurements as well as IR thermography for surface temperature measurements were used in parallel during the tests. Time-resolved capsule surface as well as aerodynamic force and moment data could be recorded. The front shield experienced significant material recessions that caused a decrease of the drag coefficient.

Index Terms— *Entry, capsule, shape change, low temperature ablator, aerodynamics*

1. INTRODUCTION

The ESA TRP MODSHAPE (Modelling Capsule Stability accounting for Shape Change) had the main goal to experimentally quantify the impact of the Outer Mould Line (OML) changes due to TPS recession on the flight qualities of capsules of potential interest to exploration missions. The team consisted of the German Aerospace Center (DLR), Fluid Gravity, Thales Alenia Space Italy and the Royal Observatory of Belgium. DLR performed experiments with models made of low temperature ablators (LTA) in the hypersonic flow regime with simultaneous in-situ recession measurements and aerodynamic stability measurements using a six-component balance.

In the past decades, the measurement of the shape change due to ablation was investigated in different studies [1]-[6], but mostly without determining the aerodynamic forces and moments at the same time. Merely, the research by Seiff et al. called attention on this relationship by analysing the entry of the Galileo probe into the Jovian atmosphere in 1995, experiencing drastic heat loads [4]. In doing so, they observed a change in frontal area of -6.9%, whereas the decrease in drag coefficient under hypersonic conditions is 2%. The information about the shape change here is taken from measurements before and after the heat loads were applied to the vehicle, which only provides an average recession rate without details about temporal behaviour. For the Mars Science Laboratory capsule, the authors propose that the shape change may be monitored by sensors locally embedded in the TPS material [1][2]. The advantage of this attempt is to gather time resolved data, but this information is limited to only local information as well as the sensors may affect the local recession of the TPS. Furthermore, Sakai mentioned an estimated accuracy for typical char sensors in the order of 1 mm [5], which are too low for recession measurement in laboratory environments. A more suitable approach is the application of optical methods in wind tunnel environments, which was demonstrated by Schairer and Heineck by the use

of a photogrammetric measurement technique [6]. The benefit of this approach is to enable a non-intrusive, three-dimensional, high-resolution measurement of the recession time history.
One main goal of the present work was to perform in-situ, temporally resolved recession measurements during the tests. Therefore, a photogrammetric approach and a Schlieren photographic approach were applied. The photogrammetric approach Projected Texture Stereo Vision (in the following called "PTSV") was identified as suitable for in-situ recession measurement in H2K. The measurement system consisted of a projector and two cameras. A specific irregular pattern is typically projected by a suitable light source in a projector in combination with suitable optics onto the object of interest. The object with patterns along its surface is synchronously captured by the two cameras of the stereo vision system. With the help of a suitable calibration of the stereoscopic camera setup and the captured measurement volume, 3D points can be rebuilt by the stereo system using a Digital Image Correlation (DIC) algorithm. For the present setup, the pattern consisted of a random arrangement of dark rectangles (like a QR-code), where the light from the projector is blocked. An example of such a pattern recorded by one of the stereo cameras is visible in right image of Figure 1-1. The commercial DIC-based software GOM ARAMIS Professional 2017 was used for the camera calibration procedure as well as the post-processing of the synchronously captured image pairs.

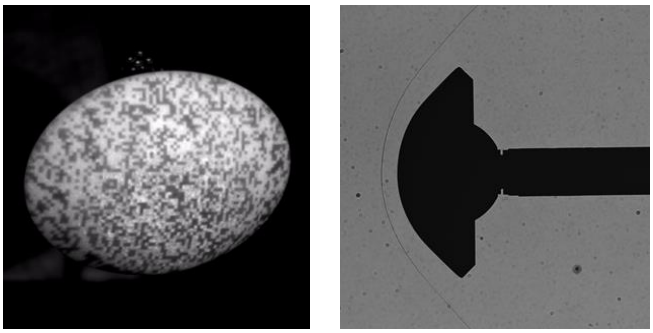

Figure 1-1: Example image of camphor-coated capsule in hypersonic flow recorded by PTSV (left) and Schlieren (right)

The approach of Schlieren photography (in the following called "Schlieren") determines a 2D profile of the contour. The measurement system consists typically of a light source, a camera and optics to manipulate the light beam. Schlieren optics systems exploit the effect of density gradients on the light propagation through a flow field. Since the contour of a model within the flow field is captured as well, the images can be used to track changes of the shape. Due to the imaging technique, only the model's line of sight contour is visible and therefore the measured shape change is typically restricted to the symmetry-plane of the model (see right image of Figure 1-1). With the help of a suitable edge detection algorithm in combination with a calibration procedure, 2D points can be rebuilt from the Schlieren images. An in-house code for Schlieren edge detection was developed by the authors.
This article begins by describing the experimental setup followed by presenting the test campaign as well as its results. Finally, a summary is given.

2. EXPERIMENTAL SETUP

2.1. Hypersonic wind tunnel cologne (H2K)

The hypersonic wind tunnel H2K in Cologne is an intermittently working blow down tunnel with a free stream test section. Since the stagnation pressure of the facility is limited to a maximum of 55 bar, the test chamber is connected to a vacuum sphere at a pressure of a few mbar to accelerate the flow to hypersonic speeds and to keep the hypersonic flow established over a long testing time. Depending on the flow condition, test durations of more than 30 seconds can be achieved. The facility is equipped with five contoured nozzles with an exit diameter of 600 mm, i.e. Mach number of 5.3, 6.0, 7.0, 8.7 & 11.2. The Mach-6 nozzle is used for this test campaign. To avoid air condensation as well as to operate the facility at high stagnation temperatures, electrical heaters of 5 MW are integrated upstream the nozzle. During the heating process the air is blown to the atmosphere until the desired stationary stagnation temperature is reached, subsequently a 3/2-way valve is activated to let the air flow through the nozzle into the vacuum dump tank. The achievable Reynolds numbers ranges between $2.0 \cdot 10^6$ m^{-1} to $20 \cdot 10^6$ m^{-1} and can be set by varying the reservoir pressure p_0 and reservoir temperatures T_0.

2.2. Wind tunnel models

Based on the discussions in [1], a modified Hayabusa probe with a reference diameter D_{ref} of 100 mm and a model scale of 1:8.8 was chosen for the present tests. The reference length for the calculation of the aerodynamic moment coefficients is the model diameter. The Moment Reference Centre (MRC) is defined at the nose (stagnation point at zero incidence angle) before the Wind Tunnel (WT) run.
Two different types of WT models with almost the same nominal dimensions were realized: The main model aimed at recession at low-enthalpy conditions and thus have an ablative surface coating. Additionally, a fixed shape PEEK capsule model was manufactured to enable reference heat flux measurements via infrared thermography and reference shape measurements. Both model geometries just differ in the shoulder shape, whereby the coated models had a round

should edge with a defined radius and the PEEK model exhibited a sharp shoulder edge. The former models consisted of a metallic model core and an ablative coating layer, which had a total thickness of 5 mm. The solid, aluminium model core was used to ensure model integrity during and after material recession and to ensure a high precision interface to the WT balance.

After a detailed review of possible candidate for the ablative coating material [1], camphor was identified as most suitable since the WT test conditions could be set in a way that the model surface pressures lie below the triple point pressure. At the same time, the triple point temperature is low enough to be overcome in H2K's test conditions but still high enough to be above atmospheric standard conditions. All essential nominal material properties of camphor are given in [1].

Prior to each WT run, a new camphor coating was sintered on the model core. For this purpose, a sintering technique was developed initially based on literature [8], [9]. As first step in the coating procedure, the raw material powder was filled into a mould that has the negative shape of the final OML contour and was compressed together with the model core. A thin layer of silicone oil in the mould supported the separation of the final model from the mould. Some iterations of coating sintering were necessary, to determine suitable conditions, which enable an almost milky white, opaque appearance of the material (see Figure 2-1). Finally, the nominal sintering pressure was set to 550 bar under atmospheric conditions, the filling mass to 44.5 g and the sintering time to 10 minutes.

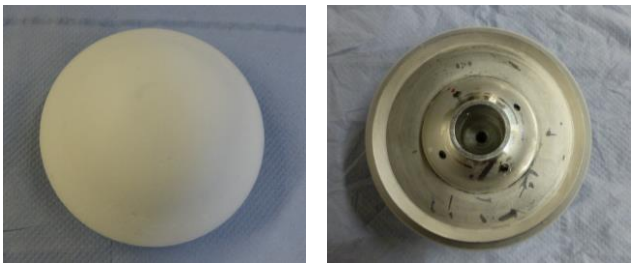

Figure 2-1: Front (left) and back (right) of finished camphor-coated capsule

Verification of the model geometry was performed with the optical high-precision profilometer Keyence VR-5200. Some exemplary surface measurements were made with the tactile high-precision profilometer Zeiss Prismo Navigator MP5/VAST as described in Section 2.4. The deviations were determined as Root Mean Square Deviations (RMSD), based on the surface-normal deviation between reference and measured contour in the vertical symmetry plane. As a result, the front-shield of an exemplary camphor-coated capsule model has a RMSD of 0.061 mm, whereby the deviation of the spherical part is generally lower than the deviation of the conical part. With a RMSD of 0.067 mm in vertical symmetry plane and 0.094 mm in horizontal symmetry plane, the RMSD of symmetry is in the same order. Taken together all camphor-coated models, a mean diameter of 100.000 mm (nominal deviation of 0.000 mm) with a standard deviation of 0.018 mm and a mean height of 47.724 mm (nominal deviation of -0.006 mm) with a standard deviation of 0.023 mm are achieved showing a very good manufacturing quality.

2.3. Wind tunnel configuration

Figure 2-2 shows the experimental setup in H2K's test section. The capsule model was placed close to the nozzle centre line at an Angle of Attack (AoA) of 0°. The model was equipped with an internal six-component balance being connected via sting to the adjustable model support, which enables the angle alignment. The PTSV system was located slightly above the nozzle exit having a view on the capsule's front-shield at an angle of roughly 40° against the horizontal plane. Additionally, an IR camera in a sealed and externally ventilated box was placed in the test section enabling a view on the model's front-shield.

In H2K, tests at non-zero AoA were also performed. Two different AoA setups with regular (up and down) as well as with sideslip (right and left) AoA mechanism were used to enable measurements with both in-situ surface measurement techniques at nonzero AoA, whereby the former setup is in the focus.

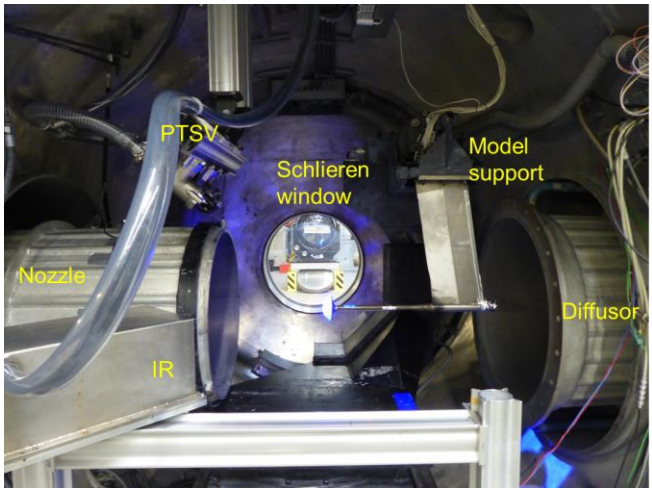

Figure 2-2: Experimental setup in H2K's test section at AoA of 0°

2.4. Instrumentation and calibration

For static force and moment measurements, the models were equipped with a six-component strain gauge balance. The balance type is a DLR inhouse design that has multiple strain gauges applied at well-defined positions to determine all three forces and all three moment components. In the nominal

balance orientation, the axial direction would correspond to x-, the normal to z-, and the pitching moment to m-component. Because the normal loads are low for blunt capsule bodies, the y- and z-component are switched for the H2K measurements. Thus, the measurement uncertainty of the balance in z-direction can be decreased due to a smaller full-scale range of the y-component. The maximum error for each component from static balance calibration is provided in Table 1. Furthermore, a low-pass filter with a cut-off frequency of 2 Hz was applied on the recorded force and moment data. The base pressure was also measured with a sensor of the UNIK 5000 series with maximal 100 mbar and a full-scale accuracy of 0.04 % (±0.04 mbar).

Table 1: Force/moment design loads and errors from balance calibration; transformations due to balance rotation: $Y_F = -Z_B, Z_F = Y_B, M_F = -N_B, N_F = M_B$

Design loads		Max. error from calibration	
X_{Bmax} [N]	200	ΔX_B [N]	±0.248
Y_{Bmax} [N]	125	ΔY_B [N]	±0.041
Z_{Bmax} [N]	500	ΔZ_B [N]	±0.065
l_{Bmax} [Nm]	5	Δl_B [Nm]	±0.011
n_{Bmax} [Nm]	6.25	Δn_B [Nm]	±0.006
m_{Bmax} [Nm]	25	Δm_B [Nm]	±0.006

For surface profile measurements in parallel to the force/moment measurement, two ex-situ and two in-situ techniques were employed to measure the recession of the model's front-shield. As ex-situ measurement techniques, an optical and a tactile profilometer were used, which measure the model contours before (pre-test) and after (post-test) the WT tests. This combination enabled a cross-check of different techniques as well as a control whether sub-surface reflection effects occur for the optical measurement techniques. As in-situ measurement techniques, the Schlieren system as well as the PTSV system were applied.

The high-precision profilometer Zeiss Prismo Navigator MP5/VAST system (in the following called "Prismo") was applied for tactile 2D surface measurements and uses a ball probe with a diameter of 3 mm.

The second pre- and post-test surface measurement was applied with the optical 3D-profilometer Keyence VR-5200 (in the following called "Keyence"), which works with structured light scanning. With several optical configurations, it can be used as macro- and microscope, enabling the measurement of surface contours and roughness.

The Schlieren system is a stationary equipment of H2K for flow visualisation and surface measurement being located outside of the test section. A z-type Schlieren photography setup (double-mirror, single-pass) without use of the knife edge (actually shadowgraphy) was applied. For the acquisition of image sequences, a 24.5-megapixel Nikon Z6 with a CMOS sensor was used. The frame rate was set to 1 Hz. The focal length of the focusing lens for image acquisition is 1000 mm. As a light source, a xenon arc lamp was utilized with a power of approximately 700 W. The Schlieren system was calibrated by the use of the fixed-shape PEEK capsule with known shape being verified by the high-precision Keyence system.

For the present tests, the PTSV system was integrated in the test section, whereby the cameras in stereoscopic arrangement and the LED pattern projector of the PTSV system were mounted on a common rail of the mounting support (see Figure 2-2). The reason for this is to enforce the cameras and the projector to experience a synchronic movement in case of vibrations and to maintain a fixed relative positioning. For the image acquisition, two iDS UI-3370CP-M-GL Rev.2 cameras with monochromic 4-megapixel CMOS sensors were used. For this camera type, a frame rate up to 5 Hz is possible. Each camera was equipped with a lens of a focal length of 35 mm and a narrow blue bandpass filter BN470, adjusted to the wave length of the projector to increase the contrast of the pattern during image acquisition. As an LED pattern projector, the 13-Watt Opto-E TRRXP-B with blue light (460 nm) in continues mode was used. Furthermore, a cloud pattern (random arrangement of dark and light rectangles) was used for the LED pattern projector having a resolution of 100 x 100 and ratio of dark to light rectangles of 35 %. The cameras were covered in sealed cases and supplied with external cooling air to prevent overheating. An arbitrary function generator HAMEG HMF2550 was used to provide an accurate trigger signal for the synchronous image acquisition. In addition, several reference marker points were attached to the balance's shroud in the field of view of the PTSV system to compensate vibrations of the sting-model-system in the post-processing and to enable the definition of an absolute coordinate system via post-processing. The calibration was performed by image recording of a differently positioned high-precision calibration plate with uncoded and coded marker points on the surface.

For the characterization, surface measurements of the PEEK capsule were performed with all recession measurement techniques under vacuum and wind-off in the test section of the H2K. Figure 2-3 shows the measured contour of the front-shield in the vertical symmetry plane in comparison to the nominal CAD contour (as described in Section 2.2). The consistent offset to the CAD contour at the nose is due to a manufacturing uncertainty. The accuracies and resolutions of the ex-situ and in-situ surface profile measurement techniques are given in Table 2. It is notable that PTSV experienced a systematic error of roughly 0.1 mm in the shown application. This was likely being caused by measuring of the distance between model's base centre and

reference marker manually with a calliper. This distance was needed to determine the coordinate system (as defined in Section 3.2) of the model contour.

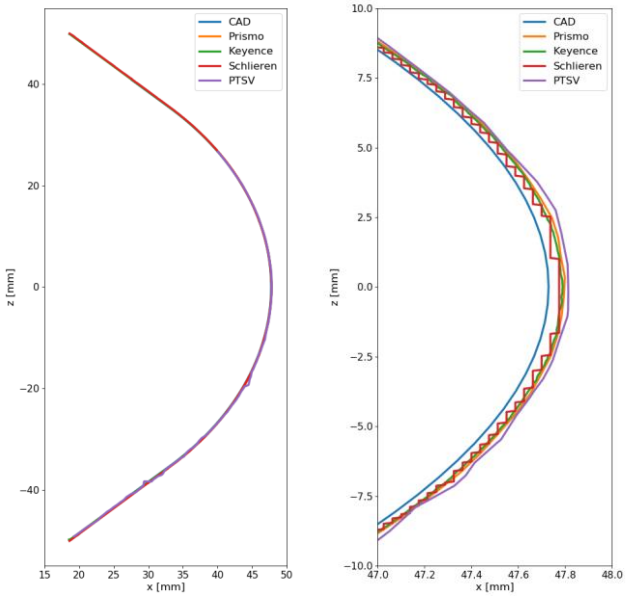

Figure 2-3: Deviation of entire front-shield (left) and nose section (right) of a PEEK capsule in the vertical symmetry plane captured with different measurement techniques in comparison to the nominal CAD contour

Table 2: Accuracies and resolutions of surface measurement techniques being used in the H2K test campaign (* values from manual)

	Keyence	Prismo	Schlieren	PTSV
Method	optical	tactile	optical	optical
Dimension	3D	2D	2D	3D
Spatial accuracy	4 µm*	1.5 µm*	72 µm	103 µm
Spatial resolution (y/z)	47.2 µm	439.1 µm	37.9 µm	373.6 µm
Spatial resolution (x)	0.1 µm*	439.1 µm	37.9 µm	N/A
Repetition accuracy	1 µm*	0.8 µm*	15.5 µm	2 µm

A VELOX 1310k SM infrared camera in combination with a 50-mm-focal-length lens was used to measure the model's surface temperature. The properties of the IR camera are given in [10]. The integration time was set to 0.1 ms for the tests with camphor-coated models covering ideally a temperature range of 20 to 125 °C. For the optical access of the sealed box, a CaF2 window was used, which has excellent transmission characteristics in the chosen IR spectral range of 1.5 to 5.5 µm. For the camphor-coated models, an overall constant emissivity of 0.94 was assumed as reported in literature [11].

3. EXPERIMENTAL TEST CAMPAIGN

Several tests were carried out in H2K with the previously described experimental setup, whereby a variation of the Reynolds number ($5.5 \cdot 10^6$ m^{-1} and $3.8 \cdot 10^6$ m^{-1}) as well as of the AoA (0°, 5° and 10°) was realized.

3.1. Test conditions

Two test conditions were applied for this test campaign as summarized in Table 3. Tests at flow conditions of H2K1 and AoA of 0° are the baseline configuration.

Table 3: Nominal H2K test conditions

	H2K1	H2K2
Mach number [-]	6.0	6.0
Reynolds number [10^6/m]	5.5	3.8
Reservoir pressure [bar]	11.33	9.50
Reservoir temperature [K]	700	800
Free-stream pressure [Pa]	709	605
Free-stream temperature [K]	85	98
Free-stream dynamic pressure [Pa]	17937.6	15218.0
Free-stream velocity [m/s]	1111.6	1187.9

3.2. Frame of reference

As shown in Figure 3-1, the Frame of Reference (FoR) is defined as body-fixed with the origin of the coordinate system in the centre of the bottom plane. The x-axis points upstream through the model nose at an AoA of 0°, while the z-axis is aligned with the gravitational vector at an AoA of 0°. α is the Angle of Attack, which describes the angle between the inflow vector and the model's x-axis. Regarding the aerodynamic coefficients, C_N is the normal force, C_A the axial force and C_Y is the lateral force coefficient; while C_l is the moment around x-axis, C_m around the y-axis and C_n around the z-axis. Unlike the coordinate system for the recession, the aerodynamic coordinate system's origin is located at the model's nose at the start of the WT run.

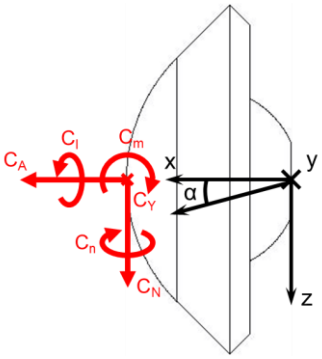

Figure 3-1: Nomenclature and coordinate system

3.3. Uncertainty analysis

The overall uncertainties of the aerodynamic force and moment coefficients were determined by applying an error propagation approach, whereby the specific uncertainties related to the error-prone input parameters were determined first by means of partial derivatives. As input, the uncertainties of the forces and moments from the balance calibration (see Table 1), the stagnation pressure sensor, the Schlieren system and therefore the diameter and finally the Mach number deviation of the Mach-6 nozzle calibrations were considered. Moreover, systematic errors due to thermal heating of the balance and the mass loss via recession during the WT tests (see Section 4.4) were also considered as an extra source of errors.

The resulting total uncertainties based on the maximum measured loads are given in Table 4. The dominant source of uncertainty is the systematic error due to thermal heating of the balance except for the axial component, which is mainly dominated by the Mach number deviation of the flow.

Table 4: Maximum total uncertainties of aerodynamic coefficients during H2K tests at H2K1 or H2K2 condition

Max. total uncertainties		
	H2K1	H2K2
ΔC_A	±0.0295	±0.0293
ΔC_Y	±0.0095	±0.0095
ΔC_N	±0.0077	±0.0077
ΔC_l	±0.0068	±0.0069
ΔC_m	±0.0049	±0.0049
ΔC_n	±0.0137	±0.0137

4. EXPERIMENTAL RESULTS

4.1. Wall temperature and reference heat flux

The wall temperature data was derived from IR thermography. In Figure 4-1, the wall temperature distribution against radial distance from the nose (s_{norm}=0) to the shoulder (s_{norm}=1) of a baseline run is shown every second of the test time, where three general findings are visible. First, the temperature decreases with increasing distance to the nose, as expected. Second, the wall temperature around the stagnation point evolves more quickly towards a limiting temperature, due to higher heat loads in the stagnation region, followed by the conical region close to the shoulder. Third, the temperatures approach a nearly constant limiting wall temperature defined by the phase change. In general, the wall temperature reaches 95% of the limiting wall temperature roughly 1 s after WT start indicating the beginning of the phase change. These observations are representative for all performed H2K tests with camphor-coated models.

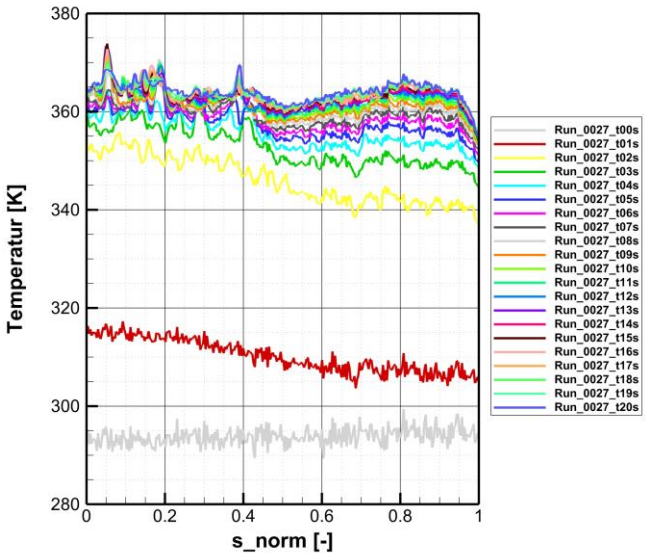

Figure 4-1: Representative wall temperature distributions on a radial line between nose (s_{norm}=0) and shoulder (s_{norm}=1) at different time steps

Since the main recession phase during a sample return re-entry is expected to occur in atmospheric heights where a laminar boundary layer along the front-shield is expected, H2K tests aimed at ensuring this boundary condition. One possibility to check for an indication of a laminar-to-turbulent transition is to check whether the wall temperature exhibits a sharp increase along typical streamlines along the wall. Apart from local spots of increased temperatures, the profiles in Figure 4-1 evolve from largest values around the stagnation point to lower values along the conical region for early test times (t < 4s). This is typical for a Boundary Layer (BL) without transition. A slight increase of wall temperatures only occurs along the conical region at a later time. But this may also be influenced by differences in camphor density and thus by the possible variability of emissivity. In consequence, it is

assumed that the BL stays laminar along the camphor model's front-shield at the selected inflow conditions.
A further check for potential BL transition is to compare measured heat flux values with laminar and turbulent computations. Therefore, a test at the higher Reynolds number condition H2K1 was performed with the PEEK model, which is a commonly used and well-characterised model material at DLR allowing 1D heat flux calculations from surface temperature data [12]. For comparison, the Harris Boundary-Layer code (BLcode) [13] was used to derive laminar and turbulent Stanton numbers. Figure 4-2 compares the experimental Stanton number distribution at different time steps to the estimated Stanton number distributions for laminar and turbulent BL against the radial distance to the nose. The Stanton numbers are in good agreement with the estimated Stanton number distribution for laminar flow (see Figure 4-2). This is a further indication for a laminar BL along the front-shield of the blunt Hayabusa shape at both selected inflow conditions, since the H2K2 condition has a lower Reynolds number.

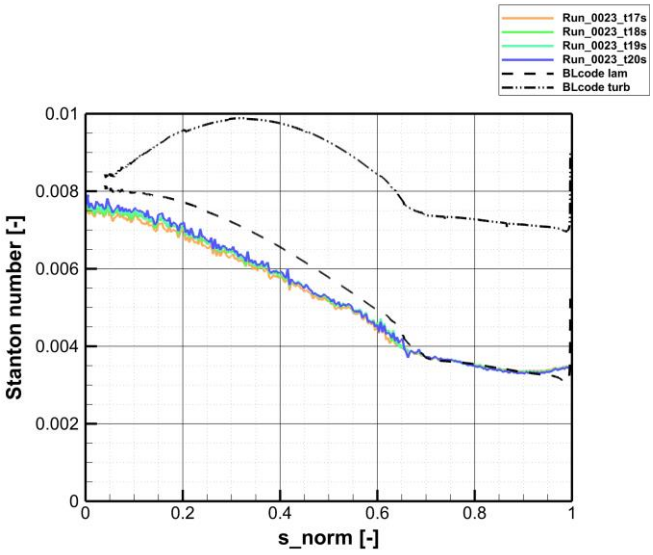

Figure 4-2: Stanton number distribution of a radial line between nose (s_{norm}=0) and shoulder (s_{norm}=1) of a PEEK model at different time steps compared to the computed Stanton number distributions with laminar and turbulent BL assumption

4.2. Impact of model coating on in-situ surface measurements

Figure 4-3 shows a comparison of contour profiles from the different techniques in the xz-plane along the front-shield of the camphor-coated capsule model before the WT run. Thereby, the result of the Schlieren method is in good agreement to the ex-situ measurements being within the uncertainties as given in Table 2. This is why no impact of the model coating on the surface measurement by Schlieren method can be identified. By contrast, deviations above the uncertainties are visible in the contour of the PTSV system (see Figure 4-3), especially in the nose region.

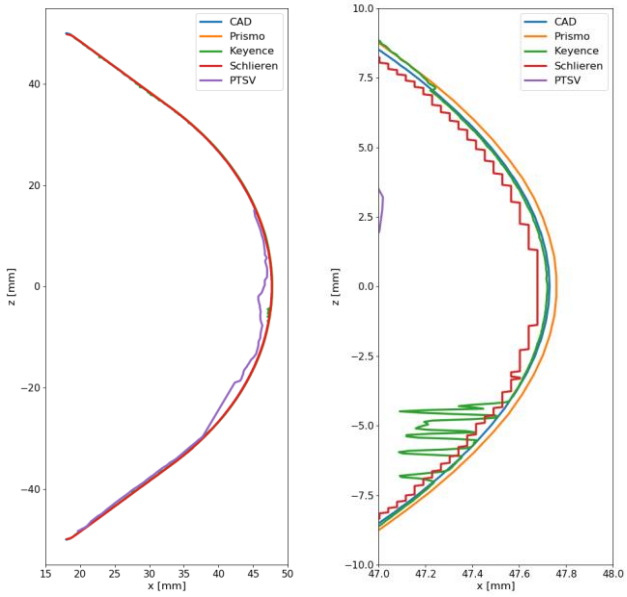

Figure 4-3: Comparison of contour profiles along front-shield (left) and nose section (right) of camphor-coated capsule model in xz-plane before WT run captured by different measurement techniques and CAD

It seems that the optical appearance of the coating has a relevant influence on the PTSV quality. For a precise surface measurement with the PTSV system, it was the aim to have a milky white, opaque appearance of the coating, because this reduced sub-surface reflections which in turn lead to higher measurement deviations. Hence, the setting of the sintering was adjusted during the pre-tests to find an appropriate combination of filling mass and sintering pressure, which enables on the one hand the aimed optical appearance and on the other hand the mechanical strength to ensure no detachment of the coating from the model core during WT run. In Figure 4-4, a camphor-coated model captured by the right camera of the PTSV system is shown before, shortly after and later after wind tunnel start. The change of sharpness appearance of the reflected speckle pattern gives an indication about the optical appearance of the coating. The pattern indicates a change of the optical appearance from translucent to opaque between a time before (0 s) and during wind tunnel start (1.2 s) and back again to translucent during the course of the run (10 s). The first transition (0 s to 1.2 s) occurs most likely due to a thin layer of oil from the sintering process (see Section 2.2), which is immediately removed at

wind tunnel start. A transition from opaque to translucent was visible during the course of all runs but it changed from run to run and was also dependent on the sintering of the capsule. Broadly speaking, a transition from opaque to translucent appears approximately 1-4 s after WT start. Furthermore, the nose region of the translucent models typically showed a higher transparency than the conical region, which could be related to the coating densities: the higher the coating density, the higher the transparency.

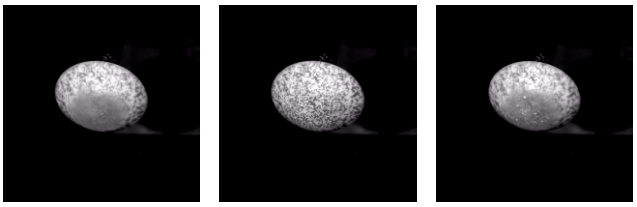

Figure 4-4: View of the right camera of the PTSV system on camphor coating exposed with LED speckle pattern at 0s (left), 1.2s (middle) and 10s (right)

To visualise the impact of this change in camphor appearance over testing time, Figure 4-5 shows a comparison of contour profiles in the xz-plane of a run at H2K1 and 0° AoA between PTSV system and Schlieren method at 0s, 1s, 2s, 10s and 25s. Since no impact of the coating appearance is expected on the Schlieren system (as previously shown), the Schlieren data is used as reference. In general, the measured x-coordinate of the PTSV system is always smaller than the one of the Schlieren method as being visible in Figure 4-5. Around 1s after Start of Recording (SoR) (almost the start of wind tunnel), the smallest deviations between both measurement techniques can be observed. For earlier times, the previously described effect of sintering oil is also visible in the contours with a larger deviation. But also for increasing testing times, the deviations are getting larger. It seems that sub-surface reflections are getting more pronounced locally with increasing testing times. This effect is more dominant in the nose region, as already shown in Figure 4-4. Therefore, the deviations of contours determined by PTSV system and Schlieren method are in order of their measurement uncertainties just during the first 1-2 s after WT start, while sub-surface reflections cannot be excluded anymore with the deviations between PSTV system and Schlieren method of up to 1-2 mm at roughly 3-4 s after WT start. As a result, the PTSV system is suitable for the measurement of reliable surface data only for the first seconds after WT start, whereas the Schlieren method should give reliable results for the complete wind tunnel run. As a consequence, the main analysis will be made based on the data of the Schlieren method in the following.

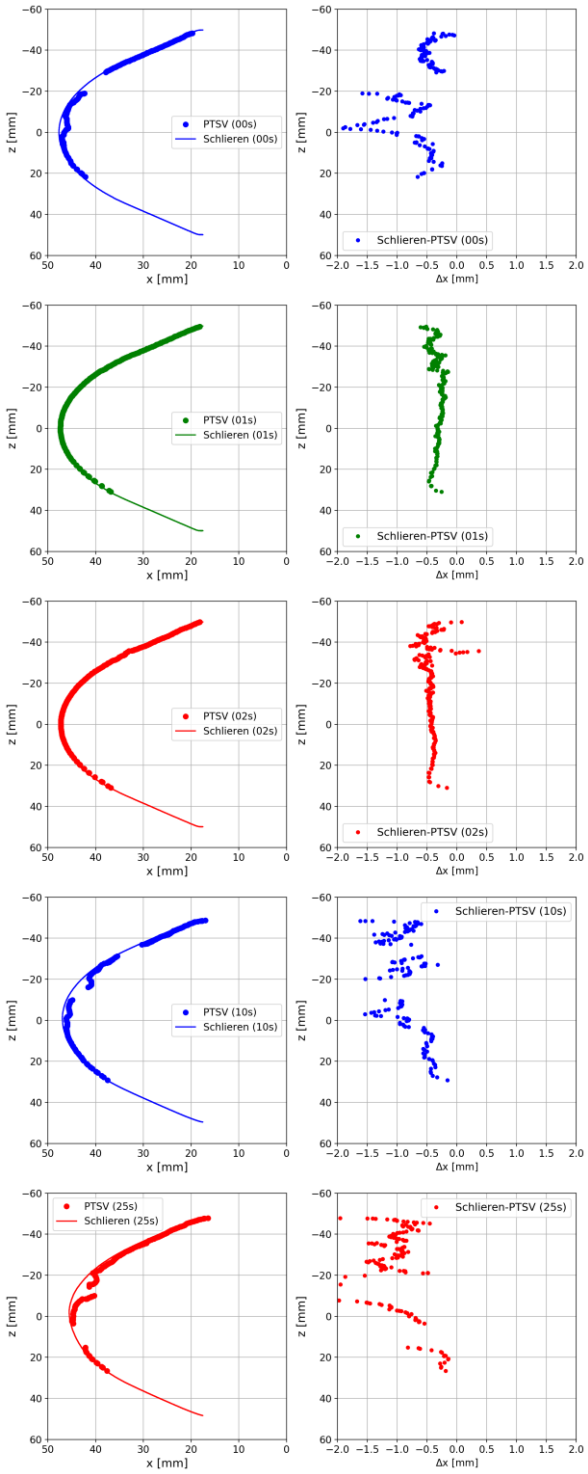

Figure 4-5: Comparison of contour profiles in xz-plane between PTSV system and Schlieren method at 0s, 1s, 2s, 10s and 25s of full front-shield (left) and deviation of PTSV system and Schlieren method (right)

4.3. Material recession

A comparison of the contour measured before and after a WT test at H2K1 and an AoA of 0° is presented Figure 4-6. It is notable that the recession depth of the spherical part is higher than of the conical part, whereby the peak recession is expected in the stagnation point of the nose. This is reasonable, because the heat flux decreases with increasing radial distance to the nose. In addition, a strong recession at the shoulder appears, partly because of local higher heat flux as well as higher shear stresses, which can cause a detachment of camphor. In general, pre- and post-test measurements indicated considerable model recessions of up to 3.4 mm in diameter, 2.6 mm in nose-to-base distance and 18 g in mass showing measurable recession under the chosen test conditions.

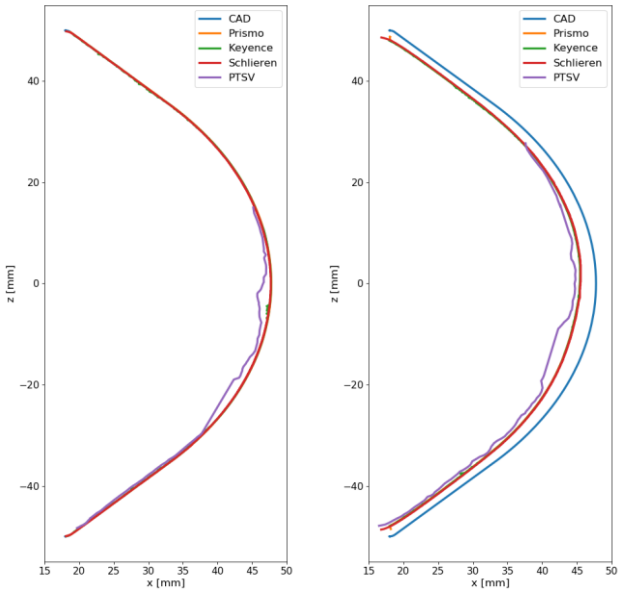

Figure 4-6: Comparison of contour profiles along front-shield in xz-plane at baseline conditions (H2K1, α=0°) before (left) and after (right) WT run by use of different measurement techniques

Differences in model mass and diameter between ex-situ (pre- and post-test) and in-situ measurement were also encountered. These apparent deviations could be attributed primarily to the recession during the evacuation of the test section prior to the WT start. A separate laboratory measurement on a camphor model under evacuated conditions of roughly 4 mbar (typical condition prior to the tests) for a representative time was performed. The camphor coating experienced a reduction in diameter between approximately 0.19 mm to 0.45 mm that is well in the range of the encountered end-of-test to post-test surface measurement differences. In contrast, the reduction in nose height between approximately 0.04 mm to 0.08 mm was within measurement uncertainties and could be neglected. The larger sensitivity to sublimation of the shoulder region can be explained by the much higher surface-to-volume ratio. To illustrate a typical temporal evolution of local recession, Figure 4-7 shows the evolution of model diameter and nose height (x-distance between nose and base centre) of a baseline run. A significant recession starts roughly 1 s after WT start (2 s after SoR). Both model dimensions show a linear decrease after start of recession until 1 s after WT shut-down (24 s after SoR). The diameter over time being measured by the in-situ Schlieren system (see Figure 4-7) has a lower value at the beginning than the pre-test ex-situ measurement and higher value at the end than the post-test ex-situ measurement. The deviations between pre-test and in-situ value with roughly 0.2 mm as well as between post-test and in-situ value with roughly 0.3 mm are beyond the measurement uncertainties of Schlieren method and Keyence system. As shown before, the residence time in vacuum is responsible for the main part of the wind-off recession. This recession is inevitable for the camphor material tests since the wind tunnel shut-down as well as pre- and post-test preparation times were already minimized. The nose height over time being measured by the in-situ Schlieren system (see Figure 4-7) shows a very good agreement with the pre- and post-test values within the uncertainties. The evolution of nose height during recession shows a linear slope over time with a recession rate of roughly 0.1 mm/s. The total recession depth at the nose is approximately 2.3 mm, here.

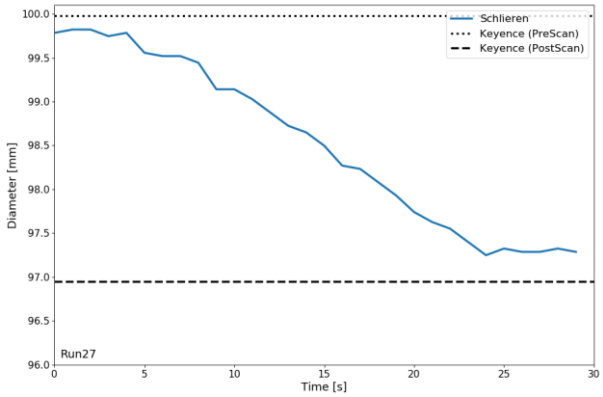

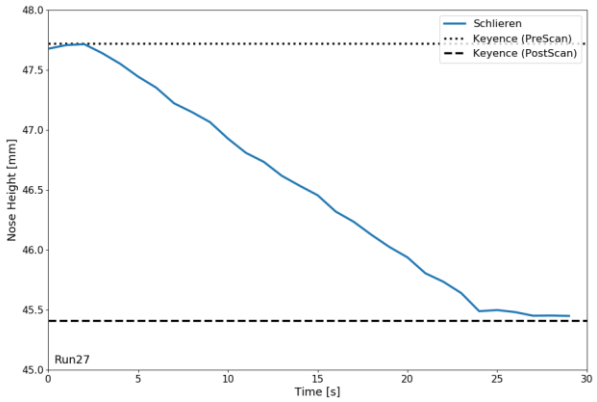

Figure 4-7: Model diameter (upper) and nose height (lower) over time at baseline conditions (H2K1, α=0°); Dotted and dashed lines feature measurement values before and after WT test

In general, a very good agreement of the contour profiles in the xz-plane can be seen in Figure 4-8 showing a good repeatability with deviations smaller than the measurement uncertainty of the Schlieren method for the H2K1 as well as H2K2 condition based on three runs for each. Figure 4-8 also depicts a comparison of the contour profile acquired shortly after WT shut-down of runs with a high Reynolds number of $5.5 \cdot 10^6$ m^{-1} (H2K1) and a low Reynolds number of $3.8 \cdot 10^6$ m^{-1} (H2K2). Apparently, the contours of runs with low Reynolds number are visible left of the contours of runs with high Reynolds number, whereby the difference decreases in the conical region. As expected, the run with low Reynolds number leads to a slightly higher recession than with high Reynolds number, due to the slightly higher total temperature (or respectively enthalpy) and lower stagnation pressure. Since most of the deviations fall below the measurement uncertainties, the Reynolds number seems to have a small impact on the change of contour profile in the tested range. The described observations regarding the Reynolds number effect were also observed for WT tests at AoA of 5°.

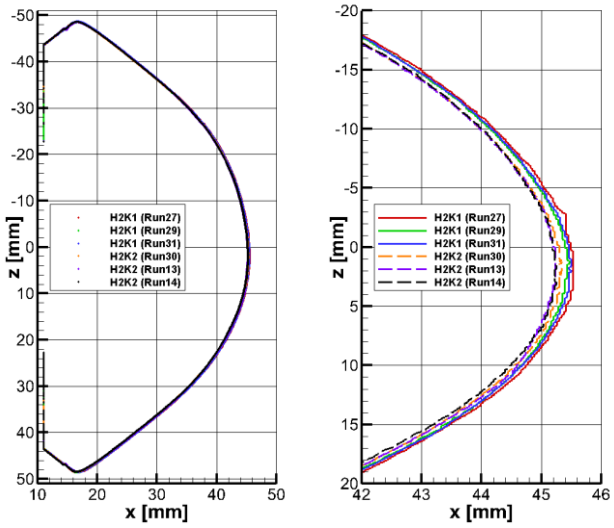

Figure 4-8: Comparison of contour profiles along front-shield (left) and nose section (right) in xz-plane after WT shut-down between H2K1 and H2K2 test condition at AoA of 0°

The contour profile in the xz-plane shortly after WT shut-down of runs with Alpha angle setup are shown in Figure 4-9 at H2K1 inflow condition as well as in Figure 4-10 at H2K2 conditions. Contours of runs with different AoA show large differences in x-positions (up to 0.6 mm), whereas the contours exhibit different shapes depending on the AoA. The repeatability of contour profiles for runs at the same inflow condition and AoA can also be shown during the tests. As expected, runs with positive AoA experience a higher recession on the lower (windward) surface than on the upper (leeward) surface, which can be seen in the conical region in Figure 4-9. Typically, along the windward side higher surface pressures and heat flux loads are expected. Furthermore, it is apparent that by increasing the AoA to 10° also the recession on the lower surface increases and the recession on the upper surface decreases for the same test condition (see Figure 4-10). Unexpectedly, for the zero-AoA runs the contour data in the close vicinity of the nose region shows a slightly higher recession along the upper surface than the lower surface (see right plot of Figure 4-9), although a symmetric recession is expected. Furthermore, the runs at AoA of 5° exhibit an almost symmetrical recession in the nose region, although a shift of the stagnation point is expected. It is not yet clear, why the recession behaviour in the close vicinity of the nose region is evident in contrast to the conical region, where the behaviour is as expected.

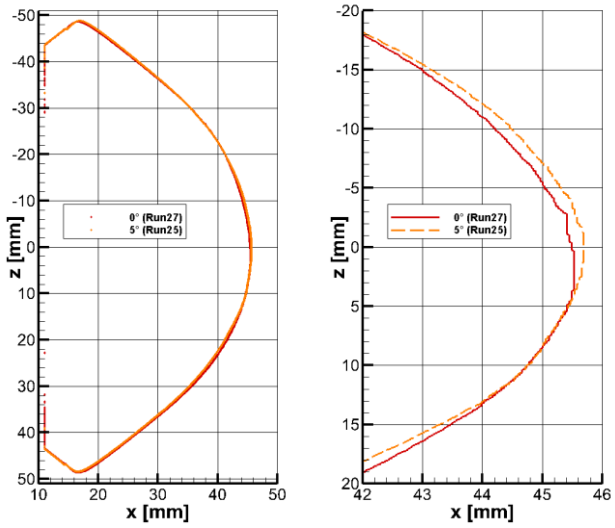

Figure 4-9: Comparison of contour profiles along front-shield (left) and nose section (right) in xz-plane after WT shut-down between AoA of 0° and 5° at H2K1

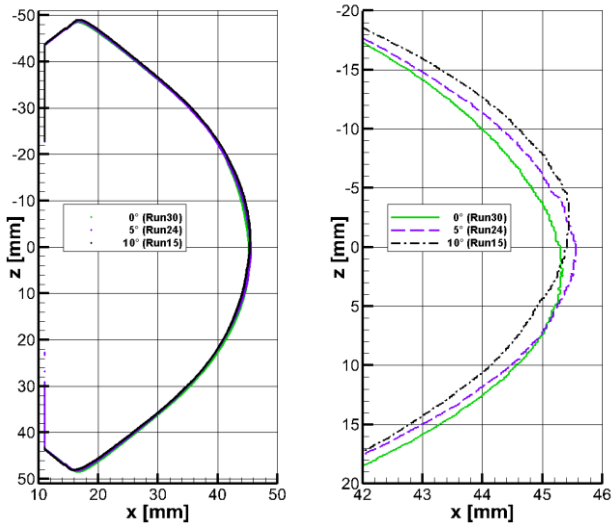

Figure 4-10: Figure 4-11: Comparison of contour profiles along front-shield (left) and nose section (right) in xz-plane after WT shut-down between AoA of 0° 5°, and 10° at H2K1

As reported before, tests at zero-AoA showed unexpected asymmetric post-test contours in the nose section (see e.g. Figure 4-9) with a RMSD value for the symmetry of 0.271 mm in the xz-plane and 0.059 mm in the xy-plane. Therefore, the RMSD value in the xz-plane has significantly changed throughout the WT test, whereas the asymmetry is more pronounced in the nose region with a RMSD of 0.345 mm in comparison to a RMSD of 0.105 mm in the conical region. In contrast to zero-AoA runs, the RMSD values for the symmetry after WT run at an AoA of 5° is acceptable with a value of 0.082 mm in the xy-plane (off-plane of the AoA). This could indicate an influence from the inflow in the wind tunnel vertical plane with a high sensitivity to the local recession.

4.4. Aerodynamic forces and moments

The aerodynamic forces and moments were measured by use of a six-component balance. However, the lateral components like rolling moment, yawing moment and side force are identical and around zero within the uncertainties, which is why they are neglected in the following analysis as well as further figures are restricted to the longitudinal coefficients and the base pressure. Furthermore, the instantaneous axial force coefficients (C_{AD}) based on the changing reference areas derived from in-situ-measured diameters as well as the fore-body axial force coefficients (C_{A_FB}) corrected by the base pressure coefficient (C_{pB}) are included in the following analysis.

Based on three runs with two different test conditions each at identical AoA of 0° as provided in Figure 4-12, a good repeatability within the uncertainties in each case could be shown for the axial force, normal force and pitching moment coefficients. The very low magnitude of the pitching moment coefficient proves symmetry and alignment of the tested configuration at AoA of 0°. In contrast, the base pressure coefficient exhibits different evolutions for test conditions with low Reynolds number (H2K2). The reason could also be a thermal effect since the pressure tube is located on the balance shroud. For the instantaneous axial force and the fore-body axial force coefficient, slight deviations are visible that are within the uncertainties though. Unlike the shown slight impact of the Reynolds number on the material recession in Section 4.3, the Reynolds number seems to have no significant impact on the aerodynamic coefficients within the given accuracies. The instantaneous and fore-body axial coefficients of both Reynolds numbers exhibit an overlapping variation, so that no clear Reynolds number effect can be identified. Interestingly, the instantaneous axial force coefficient in Figure 4-12 is roughly constant over time during all the WT runs. This indicates that the main impact on the drag force arises from the diameter and thus the surface area change.

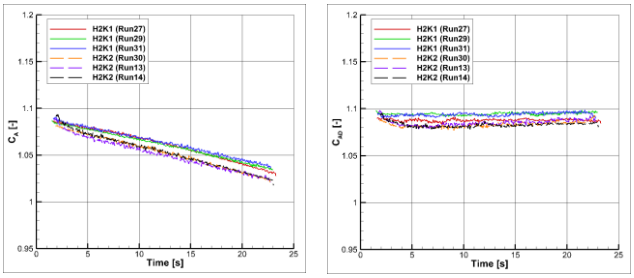

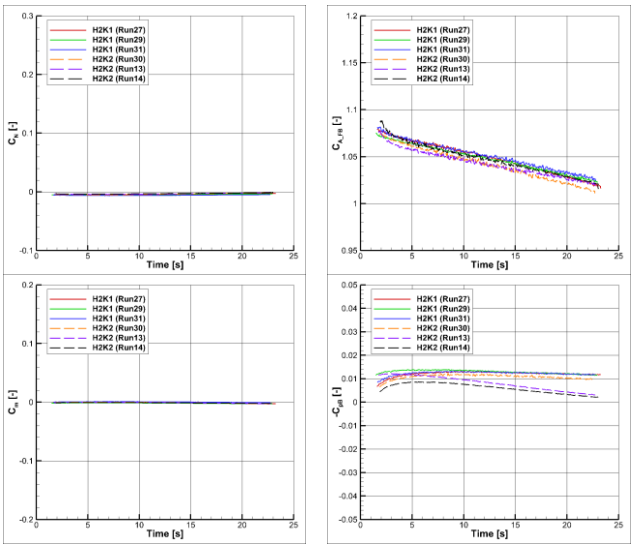

Figure 4-12: Comparison of aerodynamic coefficients at AoA of 0° between H2K1 and H2K2 condition

As a clear relationship between the AoA and the material recession could not be shown in Section 4.3, similar tendencies can be observed in the axial force coefficients (C_A, C_{AD} and C_{A_FB}) in Figure 4-12, whereby the curves at an AoA of 0° and 5° overlap within the uncertainties. Only the test at an AoA of 10° shows a significant lower axial force coefficient, as expected. For the normal force and pitching moment coefficient, a clear relation between each coefficient and the AoA is visible. The magnitude of the normal force coefficient shortly after WT start is 0.063 at an AoA of 5° and is roughly twice that value with 0.125 at an AoA of 10°. Just like the normal component, the magnitude of pitching moment coefficient shortly after WT start is 0.041 at an AoA of 5° and is roughly twice that value with 0.077 at an AoA of 10°. Both values for the normal force and pitching moment coefficients are higher than the total uncertainty of the component. Apparently, the magnitude of normal force and pitching moment coefficient slightly decrease during the WT run (see Figure 4-12), which is also an effect of the decreasing diameter. However, the instantaneous coefficients are roughly constant over time, which is why the changing normal force and pitching moment coefficient are also influenced by the diameter. The most interesting finding is that the undeformed and deformed capsule models are statically stable under the investigated test conditions.

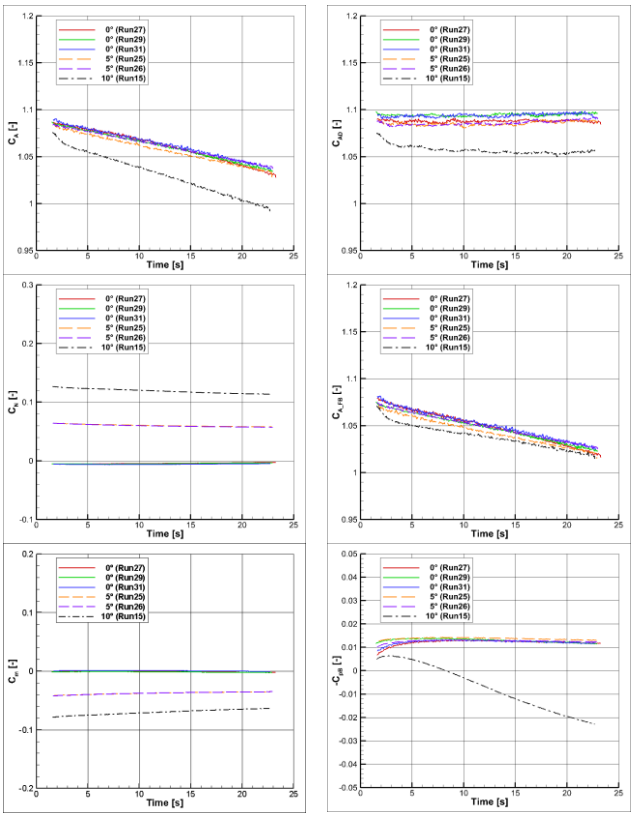

Figure 4-13: Comparison of aerodynamic coefficients at H2K1 condition between AoA of 0°, 5° and 10°

5. SUMMARY

In the present paper, the impact of shape change on static stability of a capsule in hypersonic flow was investigated. Experimental studies were therefore conducted in H2K at Mach-6 with the modified Hayabusa capsule model. A six-component balance for force/moment measurement, IR thermography for surface temperature measurement, two in-situ and two ex-situ surface measurement techniques were used in parallel in this test campaign. Thus, the measured static aerodynamic coefficients can be investigated depending on the shape change of the model. Furthermore, the study is focused on the implementation and the applicability of different surface measurement techniques for recession measurement.

The main findings of the in-situ recession measurements as well as the static stability experiments are summarized in the following:

- The PTSV system captured usable data within the measurement uncertainty for a time frame of 1-2 s after WT start. With increasing test time, the material translucency causes a sub-surface reflection of the

photogrammetric surface measurement technique PTSV leading to increased measurement uncertainties.

- The Schlieren method was able to capture the contour profile over time for all tests at AoA of 0°, 5° and 10° in regular angle setup.
- The heat flux data on the reference PEEK model and the temperature data on the camphor models indicate a laminar boundary layer along the front-shield.
- Significant material recessions during WT test occurred resulting in changes of the diameter of up to 3.4 mm, changes in the nose-to-base distance of up to 2.6 mm and changes in the model mass of up to 5% of the initial mass.
- The model diameter and nose-to-base distance decrease linearly over time during the WT runs.
- The axial force coefficient showed significant changes due to the shape change and decreases linearly during H2K runs.
- The instantaneous axial force coefficient, based on the in-situ-measured diameter, is nearly constant over time. This indicates that the main driver for the force decrease is the area reduction.
- The impact of the Reynolds number on the shape was small and only slightly larger than the measurement uncertainty. The Reynolds number had no significant impact on the aerodynamic coefficients within the given accuracies.
- The in-situ surface measurements as well as aerodynamic measurements showed good repeatability for all tested inflow and AoA conditions.
- The impact of the AoA on the shape is mostly visible in the conical region with higher recession on the lower (windward) surface, while the nose region experiences an unexpected recession due to a slightly asymmetric inflow in the region close to nozzle's centre line. The axial force coefficient curves at an AoA of 0° and 5° overlap within the uncertainties. Only the test at an AoA of 10° shows a significant lower axial force coefficient, as expected, and a larger change of coefficient during test time.
- Both the undeformed and deformed modified Hayabusa model are statically stable in hypersonic flow.

6. ACKNOLEDGEMENT

This work was performed under ESA contract 4000122733/17/NL/KML.

7. REFERENCES

[1] E. Martinez and R. Frampton, "Thermal protection system sensors", White paper to NRC decadal survey Mars subpanel and outer planets subpanel, 2022.

[2] A. Little et al., "The Mars Science Laboratory (MSL) entry, descent and landing instrumentation (MEDLI): hardware performance and data reconstruction", 36th AAS Guidance and Control Conference, Breckenridge, 2013.

[3] E.T. Schairer and J.T. Heineck, "Photogrammetric recession measurements of ablative materials in arcjets", Measurement Science and Technology, 21.2, 2010.

[4] A. Seiff, E. Venkatapathy, B. Haas and P. Intrieri; „Galileo probe aerodynamics", 14th Applied Aerodynamics Conference, New Orleans, p. 2451, 1996.

[5] T. Sakai et al., "Dual-component sensor design for in situ ablation measurement", Journal of Thermophysics and Heat Transfer, 31.2, pp. 307-317, 2016.

[6] G. Berkovic and E. Shafir, "Optical methods for distance and displacement measurements", Advances in Optics and Photonics, 4.4. pp. 441-471, 2012.

[7] D. Neeb, P. Seltner, A. Gülhan and L. Ferracina, "Modelling capsule stability accounting for shape change", International Conference on Flight Vehicles, Aerothermodynamics and Re-entry Missions & Engineering (FAR), Monopoli, 2019.

[8] A. F. Charwat, "Exploratory studies on the sublimation of slender camphor and naphthalene models in a supersonic wind-tunnel", No. RAND/RM-5506-ARPA. RAND CORP, Santa Monica, 1968.

[9] F. Lipfert and J. Genovese, "An experimental study of the boundary layers on low-temperature subliming ablators", AIAA Journal, 9(7), pp. 1330-1337, 1971.

[10] IRCAM, "Infrared camera VELOX 1310k SM Datasheet", Erlangen, 2022. https://www.ircam.de/wp-content/uploads/2021/02/IRCAM_VELOX1310kSM_10%C2%B5m_Datasheet.pdf

[11] Omega, "Table of total emissivity", Stamford, 2022. https://cn.omega.com/temperature/Z/pdf/z088-089.pdf

[12] A. Henckels and P. Gruhn, "Study on aerothermal effects of viscous shock interaction in hypersonic inlets", Fifth European Symposium on Aerothermodynamics for Space Vehicles, Vol. 563, p. 553, 2005.

[13] J. E. Harris and D. K. Blanchard, "Computer program for solving laminar, transitional, or turbulent compressible boundary-layer equations for two-dimensional and axisymmetric flow", Technical Report NASA-TM-83207, NASA Technical Memorandum, 1982.